



OPEN

Inhabited subsurface wet smectites in the hyperarid core of the Atacama Desert as an analog for the search for life on Mars

Armando Azua-Bustos^{1,2✉}, Alberto G. Fairén^{1,3✉}, Carlos González Silva⁴, Daniel Carrizo¹, Miguel Ángel Fernández-Martínez⁵, Cristián Arenas-Fajardo⁶, Maite Fernández-Sampedro¹, Carolina Gil-Lozano^{1,7}, Laura Sánchez-García¹, Carmen Ascaso⁸, Jacek Wierzchos⁸ & Elizabeth B. Rampe⁹

The modern Martian surface is unlikely to be habitable due to its extreme aridity among other environmental factors. This is the reason why the hyperarid core of the Atacama Desert has been studied as an analog for the habitability of Mars for more than 50 years. Here we report a layer enriched in smectites located just 30 cm below the surface of the hyperarid core of the Atacama. We discovered the clay-rich layer to be wet (a phenomenon never observed before in this region), keeping a high and constant relative humidity of 78% (a_w 0.780), and completely isolated from the changing and extremely dry subaerial conditions characteristic of the Atacama. The smectite-rich layer is inhabited by at least 30 halophilic species of metabolically active bacteria and archaea, unveiling a previously unreported habitat for microbial life under the surface of the driest place on Earth. The discovery of a diverse microbial community in smectite-rich subsurface layers in the hyperarid core of the Atacama, and the collection of biosignatures we have identified within the clays, suggest that similar shallow clay deposits on Mars may contain biosignatures easily reachable by current rovers and landers.

Three rovers will land on Mars in the next years (Perseverance, Rosalind Franklin and Tianwen-1) with two of them (Perseverance and Rosalind Franklin) having the primary goal of seeking preserved biosignatures in clays¹. NASA's Mars2020 *Perseverance* rover will land in Jezero crater², an impact crater with a diameter of about 45 km located at the edge of the Isidis Basin on Mars. Orbital images suggest Jezero was the site of an open-basin lake ~4 Gyr ago during the Noachian era^{3–5}. The Compact Reconnaissance Imaging Spectrometer for Mars (CRISM) onboard NASA's Mars Reconnaissance Orbiter identified iron/magnesium-smectites and magnesium-rich carbonates within the Jezero crater fan deposits^{6,7} thought to have been transported from the surrounding Nili Fossae region^{8,9} (smectites are a well-known group of phyllosilicates, or clay minerals, part of a class of “swelling clays” that can readily exchange H₂O and cations in their structures¹⁰). ESA's *Rosalind Franklin* rover will land on Oxia Planum in 2023¹¹, a Noachian terrain located on the southwest margin of Arabia Terra¹². The smectite-rich unit at Oxia is representative of a more widespread aqueously altered unit, exposures of which are found scattered over distances as large as 1900 km and which include the Mawrth Vallis clay-rich region¹³. In addition, NASA's *Curiosity* rover, which landed in Gale crater in August 2012, has already investigated an Fe/Mg smectite-bearing unit that was first identified from orbit^{14,15}.

The reason for sending rovers to smectite-bearing Martian terrains is two-fold: (1) smectite forms from water–rock interactions, and liquid water is a prerequisite for life as we know it on Earth^{16,17}, and (2) swelling clays may enable enhanced preservation of biosignatures¹⁸. On Mars, phyllosilicates are important secondary

¹Centro de Astrobiología (CSIC-INTA), 28850 Madrid, Spain. ²Instituto de Ciencias Biomédicas, Facultad de Ciencias de la Salud, Universidad Autónoma de Chile, Santiago, Chile. ³Department of Astronomy, Cornell University, Ithaca, NY 14853, USA. ⁴Facultad de Ciencias, Universidad de Tarapacá, Arica, Chile. ⁵Department of Natural Resource Sciences, McGill University, Quebec, Canada. ⁶Atacama Research, Santiago, Chile. ⁷Laboratory of Planetology and Geodynamics, Université de Nantes, 44322 Nantes, France. ⁸Museo Nacional de Ciencias Naturales (CSIC), 28006 Madrid, Spain. ⁹Astromaterials Research and Exploration Science Division, NASA Johnson Space Center, Houston, TX, USA. ✉email: aazua@cab.inta-csic.es; agfairen@cab.inta-csic.es

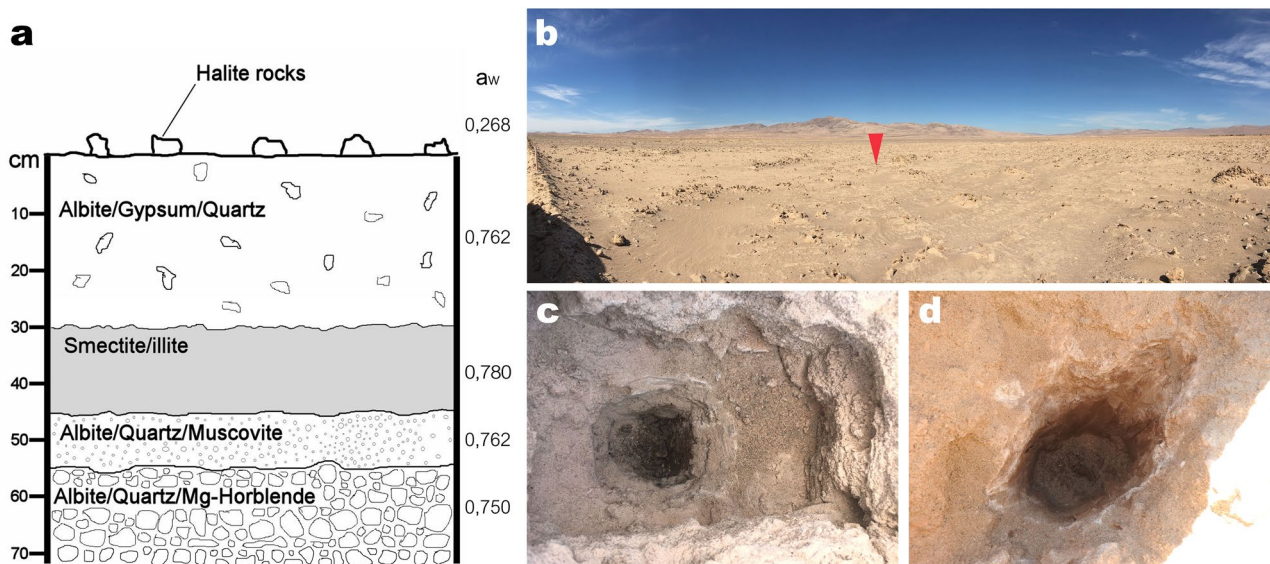


Figure 1. Characteristics of the study site. **(a)** Diagram of the structure, composition and mean water activity of soil layers with depth. **(b)** General view of the sampled site. The red arrow marks the first pit from where samples were taken, seen in detail in **(c)**. **(d)** Another pit dug 4 km away from the pit shown in **(c)**. Pit diameters are approximately 1 m length, 60 cm wide and 60 cm deep. Both **(c, d)** show a clear color change between the lower wet clay-rich layer and the upper soil layers.

minerals in ancient terrains¹⁹, with orbital and *in-situ* data indicating phyllosilicate-bearing deposits (e.g., Jezero crater, Oxia Planum, and portions of Gale crater), suggesting that past aqueous environments preserved by these deposits had a relatively high water activity and may have been habitable to microbial life^{11,16,20}. Studies of organics in smectite-bearing soils and shales on Earth demonstrate smectite can preserve organic molecules because of their reactive surfaces and ability to incorporate polar and non-polar organic molecules into the interlayer site^{21–23}. Organic molecules have been identified *in situ* in ~3.5 Gyr old smectite-bearing mudstone in Gale crater, but it is not known if and how smectite played a role in their preservation^{24,25}. Furthermore, although the surface of Mars today is unlikely habitable, the astrobiology community will be able to inspect for the first time the habitability of subsurface smectites in depth with the ExoMars Drill Unit²⁶.

The Atacama Desert, particularly the Yungay region, is a well-known Martian analog because of its hyperaridity and similar salt and phyllosilicate contents^{27–29}, and previous studies have preliminarily identified smectite in Yungay subsurface soils^{29–31}. These studies described the organic matter in smectite-rich soil horizons 10 s of cm below the surface as “fossilized” and “radiocarbon dead” and suggested the organic matter had been preserved since the time of deposition up to 2 million years ago. Although drier sites are found elsewhere in the Atacama³², Yungay is still considered one of the driest, most highly UV-irradiated environments on Earth, with highly oxidizing soils, extremely low organic content and extremely low populations of microbial life (10^1 – 10^3 colony forming units (CFU) per gram of soil)^{27,33–35}. Thus, given the critical role of smectites for preserving evidences of life, we analyzed subsurface smectite-rich soil horizons in pits dug in the hyperarid Yungay region (Fig. 1) in order to characterize its environmental conditions, assess its habitability and its potential for preserving biosignatures.

Results and discussions

Our first observation in the studied area took place in the second week of March 2017, while sampling soils in a pit dug in the middle of Yungay (24°5′5.28″S, 69°54′54.25″W) (Fig. 1a,b). Starting 30 cm below the thoroughly characterized halite, gypsum, albite and quartz-rich soil surface and shallow subsurface^{36–38}, we observed a distinct layer of wet clay mineral-rich soil (Fig. 1c). These wet sediments were also observed in the same pit later in March, July and August 2018. Four additional pits dug in August 2018 in a 4 km radius around the first pit also unveiled wet clay-rich soils in the subsurface (Fig. 1d), confirming the existence of a widespread and sustained phenomenon of sub-surface water availability at Yungay. To the best of our knowledge, this represents the first detection of wet subsurface clay-rich layers (or any other type of subsurface wet minerals) at Yungay or other sites of the hyperarid core of the Atacama.

Standard gravimetric analyses of the wet clay-bearing layer confirmed they comprise 42.8 wt% consist of clay size particles. Both X-ray diffraction (XRD) of oriented clay-size ($< 2 \mu\text{m}$) aggregates and near-infrared spectra of these same samples unveiled interstratified illite–smectite as the main clay component (Fig. 2). XRD of the clay-size fraction also demonstrated the presence of discrete illite and chlorite. Samples collected from the wet clay-bearing layers also contain halite (NaCl), gypsum ($\text{CaSO}_4 \cdot 2\text{H}_2\text{O}$), calcium carbonate (calcite, CaCO_3), albite ($\text{Na}(\text{AlSi}_3\text{O}_8)$) and quartz (SiO_2) (Supplemental Figure S1), all minerals typical of surface soils in this area^{39–41}.

Dual temperature/relative humidity loggers buried in the soil profile (at the surface, 20 cm and 40 cm below the surface, this last sensor set in the middle of the clay layer) in the first inspected pit in 2018 and 2019 showed that while atmospheric relative humidity widely fluctuated daily (as it usually does in the hyperarid core of the Atacama)^{32,42}, relative humidity deeper in the soil profile always remained high and constant over time (Fig. 3a).

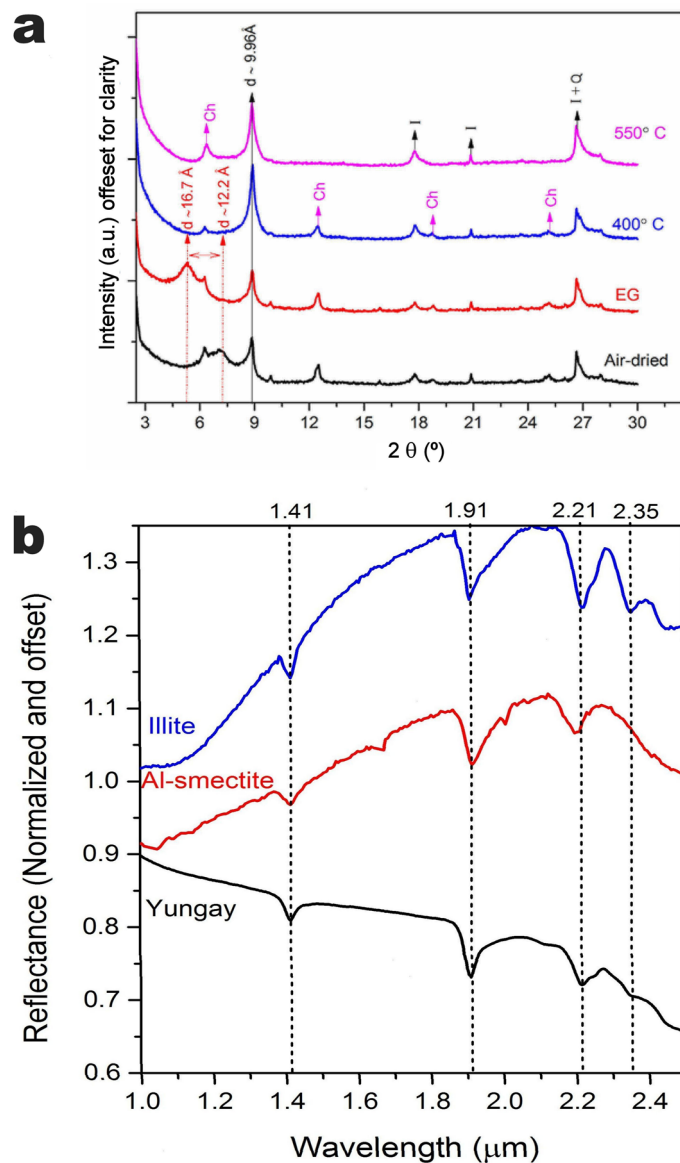


Figure 2. Mineralogical characterization of Yungay clay-size separates. **(a)** From bottom to top, XRD patterns of an oriented clay mount following a step-procedure to identify clay minerals: air-dried, glycolated and heated at 400 and 500 °C. The presence of a broad peak at 12.2 Å which migrated at 16.7 Å in the glycolated pattern and the presence of reflections assigned to illite (I) point to an interstratified illite-smectite specimen. The perpetuation of a sharp peak at 10 Å in all patterns indicates discrete illite is present. The sample also contains chlorite and quartz (Ch and Q). **(b)** Near-infrared spectra of Yungay clay-size separates. From bottom to top, near-infrared spectra of Yungay clay-size separate (“Yungay”), Al-smectite (montmorillonite, from CRISM spectra library) and illite (from PDS Geoscience spectra library). The Yungay clay spectrum shown is an average of three independent measurements (64 scans, 2 cm⁻¹ of resolution), normalized by the maximum intensity. Dotted lines mark the vibrational bands of the clay minerals: 1.41 and 1.91 μm assigned to the combinations and overtone vibrations in OH and H₂O; vibrational bands between 2.1 and 2.5 μm result from the distribution of cations in octahedral sites, and the bands at 2.21 μm and 2.35 μm are consistent with Al–OH and Fe–OH, respectively.

The sensor set 20 cm below the soil surface showed some variations in relative humidity (Fig. 3a), reflecting a small influence of atmospheric changes in the soil at this depth. However, the sensor set in the clay-rich layer, 40 cm beneath the soil surface, showed a high relative humidity of 78.0% (a_w 0.780), which remained constant for the measured time periods (see Methods). This value is much higher than the highest a_w values reported in Yungay surface soils, which typically vary between 0.01 and 0.524, and well above the lowest water activity limit for microbial life (a_w 0.6)³². The temperature profile over time showed that the clay-rich layer is also thermally independent of the surface atmospheric conditions (Fig. 3b); temperatures on the soil surface varied amply between 0 and 54 °C depending on the time of day, while the sensor at a depth of 20 cm fluctuated between 14 and 19 °C. In contrast, the sensor set in the clay-rich layer at a depth of 40 cm maintained a constant temperature

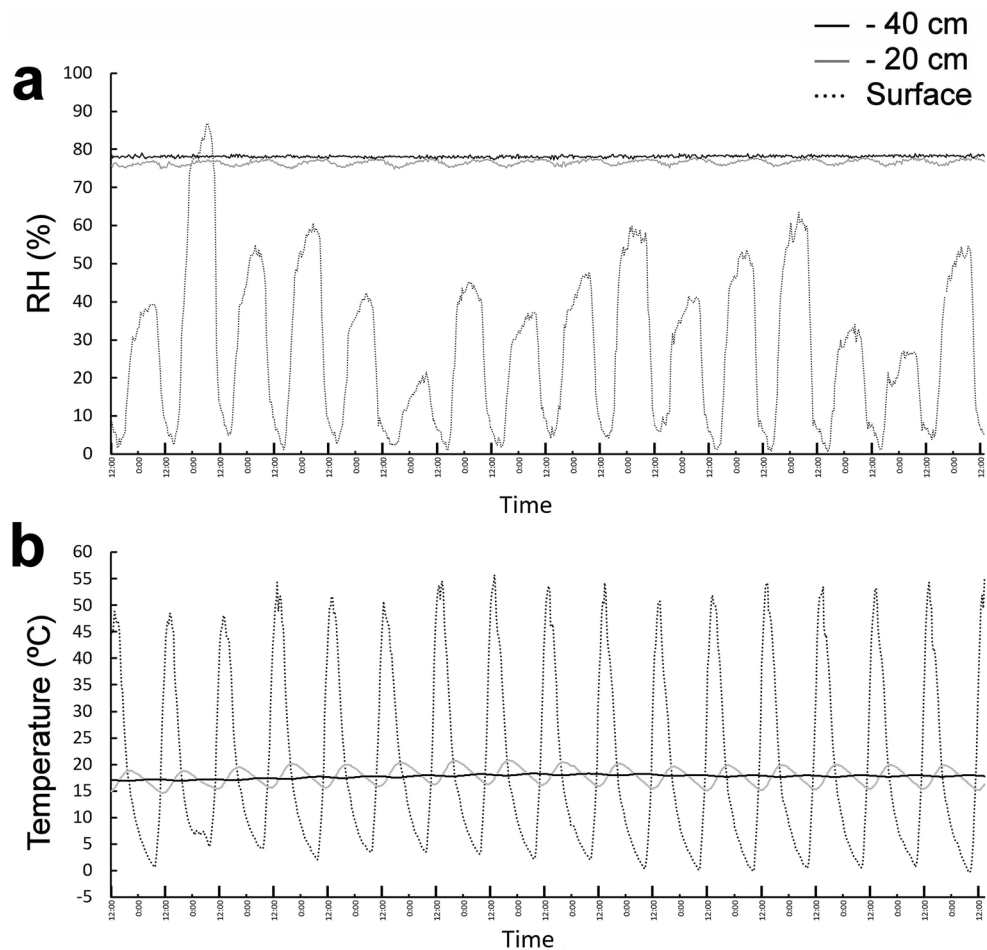


Figure 3. Temporal behavior of relative humidity and temperature in Yungay soil profile. **(a)** Relative humidity changes over the course of 16 days. **(b)** Temperature changes over the same time period as **(a)**. Larger marks in the x axis show noon time of each day.

around 17 °C, with only minor variations over time (± 1 °C). A statistical analysis of the influence of atmospheric surface temperatures on surface relative humidity in the soil profile confirmed our observations: temperature and relative humidity at the surface show a strong inverse correlation (Supplemental Figure S2, panel a). Relative humidity at a depth of 20 cm showed a minor negative correlation with atmospheric surface temperatures (Supplemental Figure S2, panel b), while within the clay-rich layer at a depth of 40 cm, relative humidity was almost completely uncoupled from the harsh and changing surface conditions (Supplemental Figure S2, panel c).

Below the clay-rich layer, we found another layer composed of granular material (a_w 0.762), mainly containing albite (calcian), quartz and orthoclase; and, below this, a hard, rocky stratum (a_w 0.750) composed of albite (calcian), quartz and ferrous magnesiohornblende (Fig. 1a). The minor decrease in water activity of the layers below the clay-rich layer shows that the illite–smectite in the clay-rich layer preferentially holds water, but may also provide a source of humidity for layers below it. Standard gravimetric analyses^{43,44} of the illite–smectite-bearing samples showed that these clays hold up to 20% of their weight in water available for microbial life. The source of water for the wet subsurface clay-rich layer is likely related to unusually intense rain events in Yungay over the past decade, particularly in March 2015 when the region received ~ 35 mm of precipitation over the course of several days⁴⁵. Later rain events even created small lagoons in Yungay in 2017, a phenomenon never observed before in this region in the past 500 years⁴⁶.

Although the exact environmental conditions on early Mars are largely unknown, similarities in mineralogy between soils at Yungay and Noachian- and Hesperian-aged Martian terrains indicate similar conditions to those in Yungay soils may have existed on early Mars. Sulfates and chlorides have been detected from orbit and in situ by rovers and are generally indicative of arid and evaporative environments^{47,48}. Many of these salts are located in depressions or impact craters and can be associated with clay minerals^{49,50}. Saline waters may have been sourced from groundwater upwelling and/or surface runoff, but the identification of river and delta deposits in some of these craters suggests surface runoff was a factor in these locations, and lake level sequences in Gale crater indicate multiple drying and rewetting cycles⁵¹. Arid, evaporative environments, indicated by sulfates and chlorides, and local flooding from surface runoff, perhaps from melting snow and ice in the case of early Mars, followed by periods of aridity likely existed on early Mars as they do now at Yungay.

Clay-rich layer samples showed a total organic content of 0.10% dry weight (dw) (a value ten times higher than the highest organic surface carbon values measured in Yungay)^{44,45}, and total nitrogen of 0.01% dw, resulting in a C/N ratio of 10, a value in the higher limit range of other reports of desert microbial biomass⁴⁶. Stable isotopic ratios were -23.4‰ ($\delta^{13}\text{C}$) and 2.3‰ ($\delta^{15}\text{N}$). Depleted bulk $\delta^{13}\text{C}$ ratios suggest that primary carbon fixation in these wet clay-rich layers may be explained either by a subsurface acetyl-CoA pathway (bacteria and/or archaea) and/or by the downward transport of Calvin cycle products created at the surface, as endolithic metabolically active cyanobacteria have been reported inside halites of the surface of the sampled area^{38,40,52}.

Although the heterogeneous distribution of cells in small colonies in the clay samples analyzed complicate the assessment of microbial colonization in this new habitat, we have estimated population levels of at least 9.3×10^3 cells per gram of sample using direct counting after SYBR Green staining. Fluorescence microscopy analysis of clay-rich samples from 40 cm depth stained with SYBR Green also revealed that microbial cells in these clay minerals form discrete, isolated colonies encapsulated by an envelope of exopolysaccharides similar to biofilms (Fig. 4a–d), suggesting a functional collaboration among these cells⁵³. In addition, CTC (5-Cyano-2,3-di-p-toly tetrazolium chloride, a redox dye commonly used as cellular indicator of respiratory activity) staining of these same samples clearly showed that these cells are actively respiring, demonstrating that these colonies are metabolically active (Fig. 4e,f), and not in a state of metabolic stasis, as it has been proposed in general for microbial species found in subsurface soils of the hyperarid core of the Atacama⁵⁴.

We used culture-dependent and culture-independent methods to investigate the habitability of the wet clay-rich soils identified at Yungay. Direct DNA extraction and the subsequent massive parallel sequencing of 16S ribosomal RNA gene amplicons showed that the majority of the sequences obtained are phylogenetically close to 30 bacterial and archaeal species (Fig. 5a), thus unveiling a microbial diversity higher than that reported for soils of this area^{30,40,55}. We found that the highest diversity of species was among the Actinobacteria (i.e., *Kocuria*, *Arthrobacter* and other uncultured species of unknown affiliation), followed by halophilic archaea (*Halostella*, *Natromonas*, *Halorussus*, *Natrinema*), beta- (*Undibacterium*, *Aquabacterium*, *Massilia* and *Ralstonia*) and gamma-proteobacteria (*Acinetobacter johnsonii*, *Halomonas gudaonensis*, *Marinimicrobium locisalis*), with a few species of Firmicutes (*Anaerococcus*, *Lactobacillus*, *Tepidibacter*, *Streptococcus*), cyanobacteria (*Halothece*) and Bacteroidetes (*Salinibacter*). Some of these species have been already reported in Yungay soils and other regions of the Atacama, such as *Halothece*⁵⁶, *Corynebacterium*^{57,58}, *Kocuria*⁵⁹, *Lactobacillus* and *Streptococcus*^{60,61}, *Anaerococcus*⁶², *Halomonas* and *Salinibacter*^{38,58,62}. Interestingly, we recently reported *Halomonas gudaonensis*, *Marinimicrobium locisalis* and *Acinetobacter johnsonii* as three of only four microbial species able to reproduce in the extremely rare temporary lagoons that formed after the very unusual rains in Yungay in 2017⁴⁶. This suggests that both ecosystems (subsurface clay soils and surface lagoons) were temporarily connected (temporarily, as these lagoons had completely evaporated at the time of our latest pits dug on 2018), thus suggesting that these three microbial species may have originated from the subsurface wet clay soils reported here. The analyses of microbial species in these lagoons showed that high rainfall events annihilated most surface species in Yungay⁴⁶, however, the diversity of microorganisms in the wet clay-rich soils suggests that the subsurface microbial community in Yungay thrives or at least remained unaffected following high rainfall events. Cultivation of clay-rich samples in different growing media allowed the growth of 23 novel halotolerant bacterial isolates (Fig. 5b), with many species phylogenetically close to genera not detected by direct DNA extraction, such as *Oceanobacillus*, *Lysinibacillus*, *Virgibacillus*, *Halobacillus* and *Bacillus*. Similar to the species detected by direct DNA extraction from clay-rich samples, the microbial species found by cultivation also match the halotolerant/halophilic species reported by other authors in Yungay, like *Halobacillus*⁶³; and also other surface and subsurface soils in the Atacama (*Halobacillus*, *Virgibacillus*, *Oceanobacillus*, and *Bacillus*⁶⁴). The case of *Bacillus* spp. is worth mentioning, as species of this genus are among the first and one of the most common type of bacteria reported in Yungay^{27,65,66} and also in other sites of the hyperarid core of the Atacama^{67–69}.

With the aim of helping inform decisions for the upcoming inspection of Martian smectite by NASA and ESA rovers, we also analyzed what type of biosignatures could be detected in the inhabited wet subsurface smectites of Yungay (Fig. 6a–c). The lipid analysis from clay-rich samples confirmed the presence of microbial biosignatures (heptadecane and phytol derivatives) typically associated with different microorganisms such as sulfate-reducing bacteria (*iso/anteiso* carboxylic acids), archaea (squalene and crocetane), green non-sulphur bacteria and interestingly, also, cyanobacteria (Fig. 6a,c). Thus, these results not only unveiled the biosignatures produced by the microbial species that inhabit the subsurface clay minerals reported here, but also the molecular remains produced by the microbial species reported in the halites present on the surface^{40,70,71}. This is the case of *Halothece* (also detected through Next Generation Sequencing; NGS), of particular interest because it is the only cyanobacteria reported inside halites on the surface soils of Yungay⁷¹ (the presence of cyanobacteria in the inspected clay-rich samples is ruled out as light does not penetrate 40 cm below the surface, see Supplemental Table S1). The detection of biosignatures of this cyanobacterium on the clay layer lends additional support to the hypothesis that primary carbon fixation in this community can be at least partially explained by the downward seepage of Calvin cycle products synthesized at the surface.

Iso/anteiso pairs of the C_{15} and C_{17} *n*-carboxylic acids were relatively abundant in the acidic fraction of the analyzed clay-rich samples (Fig. 6a), consistent with the species reported by NGS sequencing. These are lipidic components characteristic of sulphate-reducing bacteria membranes^{72,73} also found in heterotrophic bacteria such as *Thermus*, *Deinococcus* or *Bacillus*⁷⁴. The detection of monounsaturated carboxylic acids such as 16:1 ω 7; 16:1 ω 9 or 18:1 ω 9 are also related to the presence of phototrophic bacteria^{74–76}. The dominance of the C_{17} chain within the low molecular-weight *n*-alkanes (Fig. 6c) and the presence of branched (mostly mono-methylated) *n*-alkanes supported the presence of cyanobacterial sources too^{77–80}, as previously described in other surface sites of the Atacama^{46,80}. The detection of pristane and phytane also supports the input from surface cyanobacteria, as both isoprenoids are widely viewed as transformation products of phytol⁸¹. However, other than cyanobacterial origin, pristane can also be sourced in plants or phytoplankton⁸², and phytane can be sourced

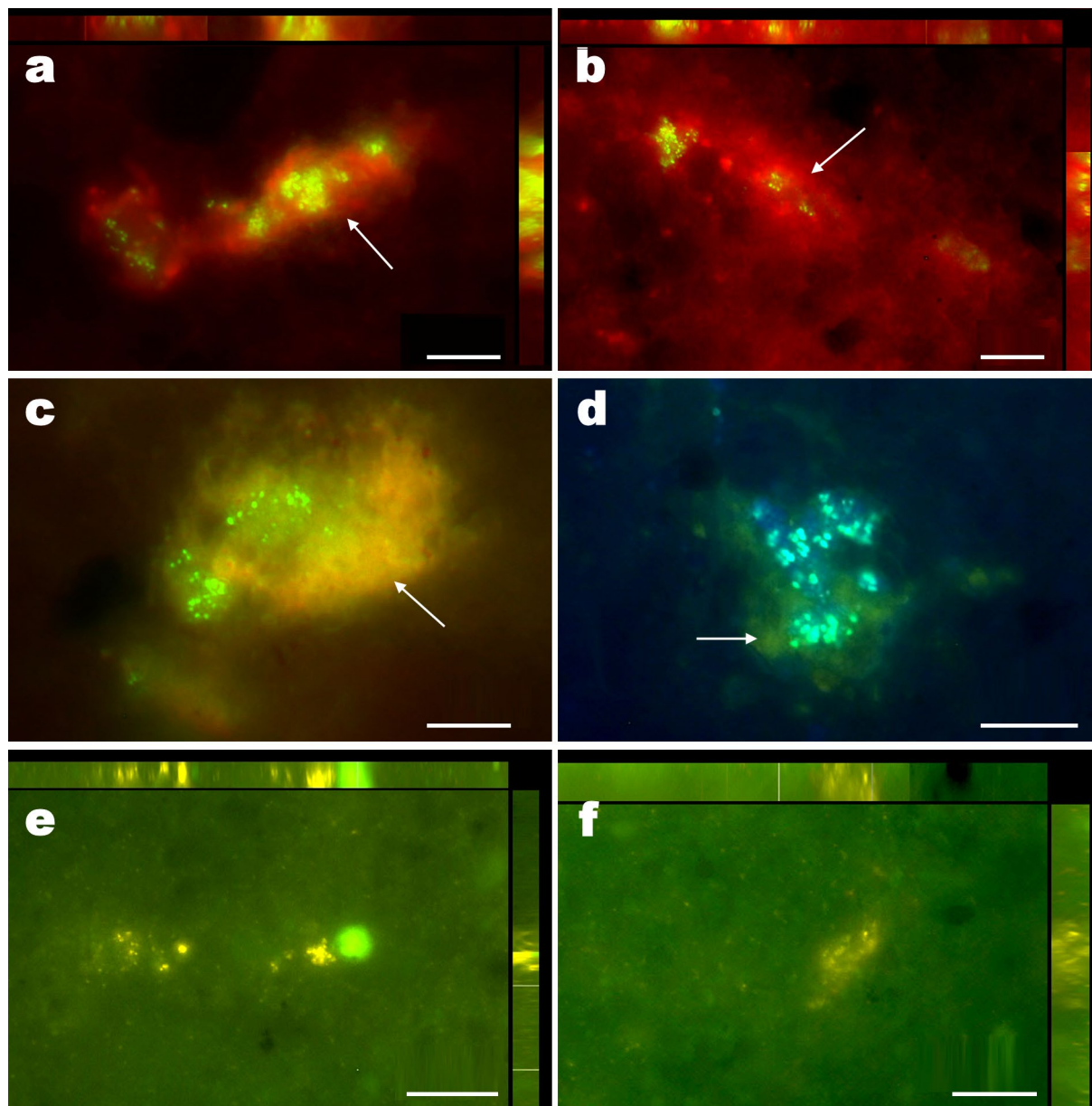


Figure 4. Fluorescence microscopy images of bacterial aggregates and EPS from Yungay subsurface clay samples. **(a, b)**, Maximum image projection 3D images (upper and right bars: X and Y view of stacked sections respectively, 10 sections; $z = 0.35 \mu\text{m}$) of SYBR green stained bacterial cells (green-yellow signal) and autofluorescence red signal (arrow), potentially proceeding from exopolysaccharides. The sGFP and Rhodamine filters were used for both images (Multichannel Image Acquisition system). **(c)** Single section image of SYBR green stained bacterial cells (green signal) and autofluorescence orange (arrow) signal potentially proceeded from EPS; sGFP filter. **(d)** Single section image of SYBR green stained bacterial cells (blue signal) and autofluorescence green (arrow) signal potentially proceeded from EPS; DAPI filter. **(e, f)**, Maximum Image Projection 3D images (upper and right bars: X and Y view of stacked sections respectively, 10 and 15 sections respectively; $z = 0.35 \mu\text{m}$) of CTC stained and metabolically active bacterial cells (yellow-orange CTF signal).

in archaeol, the most commonly reported core lipid in archaea^{31,83}. The contribution from archaea may also be inferred from the presence of squalene and crocetane (although squalene can also be synthesized by fungi), other isoprenoids characteristically attributed to halophilic^{84,85} or methanogenic/methanotrophic⁸⁵ archaea, in line with the archaeal species found by NGS sequencing. In addition to the dominant microbial biomarkers, a contribution from eukaryotes was also inferred from the detection of certain terrestrial lipid biomarkers such as stigmastanol^{86,87} (Fig. 6b) and odd high molecular-weight *n*-alkanes (i.e. C27, C29, and C31^{88,89} (Fig. 6a,c). Because these are highly recalcitrant biomolecules, able to resist decay even for billions of years⁸³, and considering that the samples were collected at 40 cm depth, their presence may be potentially explained by the aerial input of allochthonous material coming from elsewhere in the distant past^{30,69,80}. The aerial transport of such recalcitrant biomolecules have been described in the Atacama in places such as the neighboring Salar Grande⁸⁰ and in other

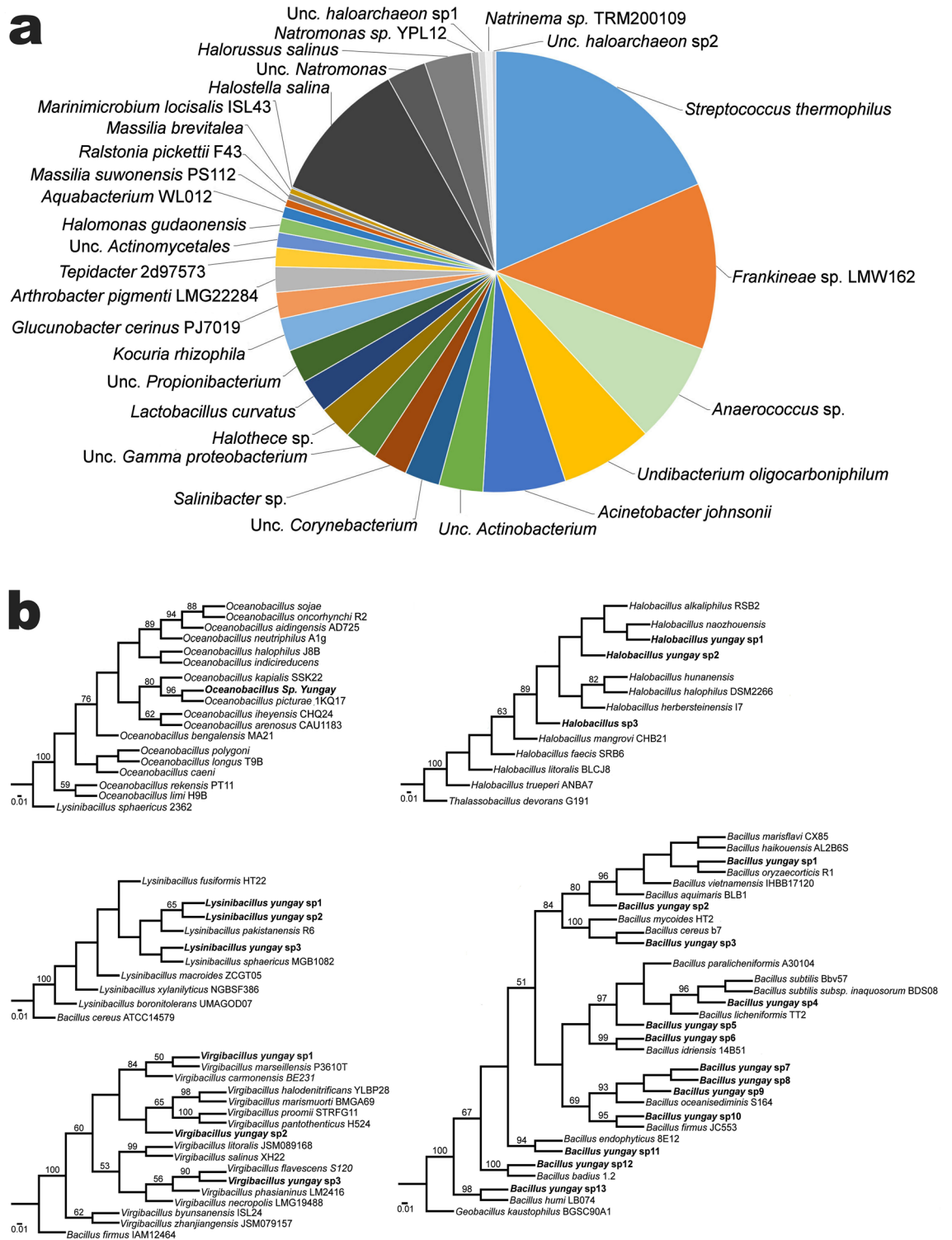


Figure 5. Closest phylogenetic matches of the microbial species identified in Yungay subsurface clay minerals. (a) Main OTUs identified from DNA extracted from Yungay subsurface clay samples. Wedges in gray denote archaeal species. (b) Phylip neighbor joining phylogenetic trees obtained from the aligned 16S rRNA gene sequences of clay microbial isolates (*Oceanobacillus*, *Halobacillus*, *Lysinibacillus*, *Bacillus* and *Virgibacillus*) and related species. Numbers on the nodes represent bootstrap values with 10,000 replicates. Phylogenetic trees were done with the freely available Bosque Phylogenetical Analysis Software version 1.7.152, <https://bosque.udec.cl>.

polyextreme hydrothermal environments such as Dallol in Ethiopia⁸⁵. Altogether, the lipid analysis revealed presence of microbial biomarkers produced by the microorganisms inhabiting the subsurface illite–smectite and

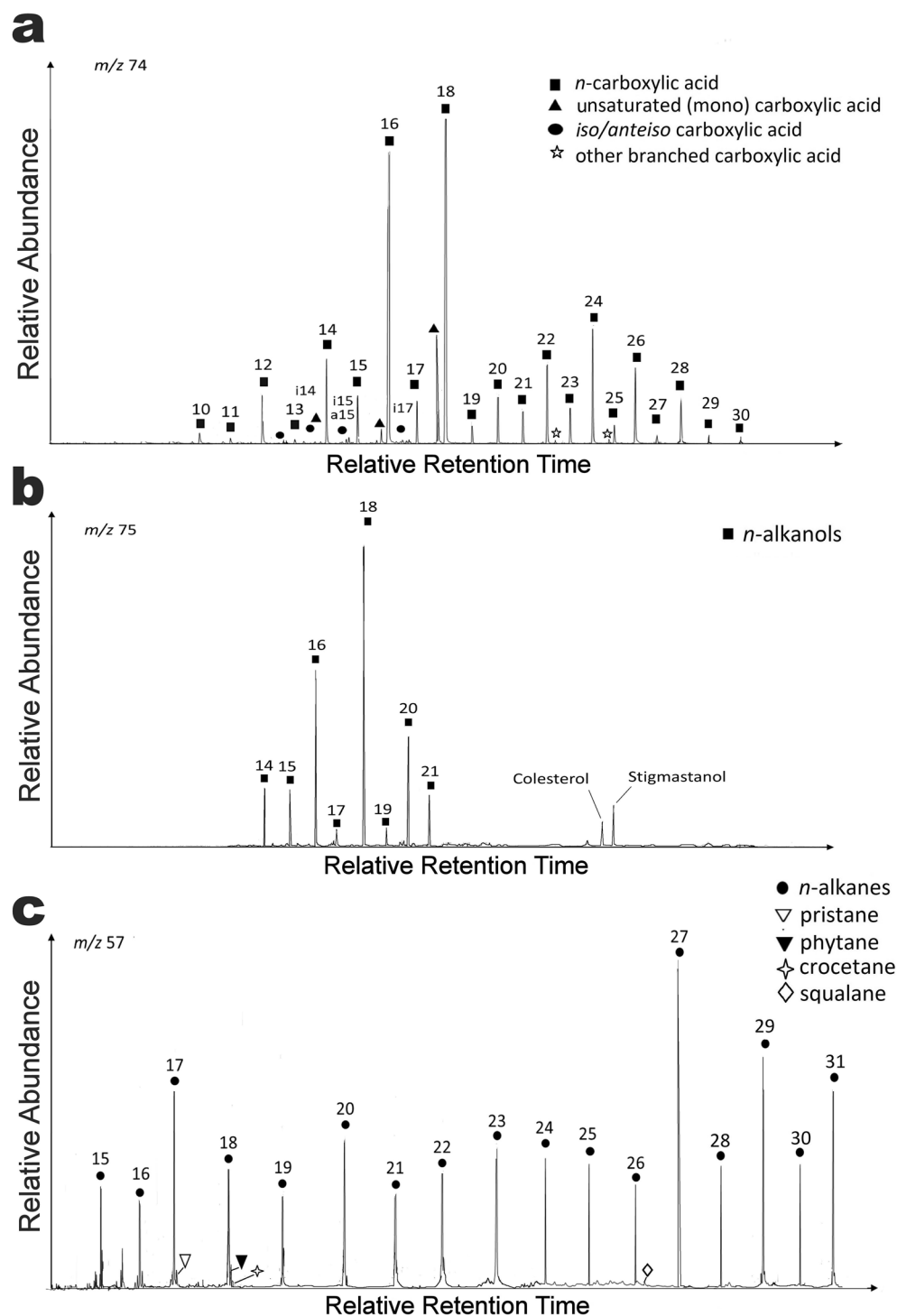


Figure 6. Mass chromatograms of the three major lipid families in Yungay subsurface clay samples. (a) Carboxylic acids as methyl esters (*m/z* 74). (b) *n*-alkanols as trimethyl-silyl esters (*m/z* 75). (c) *n*-alkanes (*m/z* 57).

those inhabiting surface halites^{40,56,71}. The use of source-specific lipid biosignatures in these samples allowed us to elucidate the structure of the microbial community and the different carbon assimilation pathways operating in the clay-rich microenvironment. As already mentioned, the biomass isotopic ratio of $\delta^{13}\text{C}$ measured in the clay-rich microenvironment. As already mentioned, the biomass isotopic ratio of $\delta^{13}\text{C}$ measured in the biomass (i.e., TOC) of the clay-rich samples was -23.4‰ . Assuming a mean $\delta^{13}\text{C}$ of -8‰ for the fixed atmospheric CO_2 ^{90,91}, the observed $\delta^{13}\text{C}$ value corresponded to a fractionation of *ca.* 15‰, which is within the range ($\delta^{13}\text{C}$ from -11 to -26‰) of those described for microorganisms assimilating CO_2 by the Calvin cycle⁹². A depletion of $\delta^{13}\text{C}$ at C_{17} (-28.4‰) compared to that at C_{16} (-26.5‰) or C_{18} (-27.0‰) suggests a different source for

C₁₇ homologue relative to the other two low molecular-weight *n*-alkanes. The dominance of C₁₇ among the low molecular-weight *n*-alkanes (Fig. 6) is likely related to an input source of cyanobacteria^{81,93,94}. $\delta^{13}\text{C}$ compound specific isotope analysis for higher *n*-alkanes (C₂₇ and C₂₉) rather reflects a possible eukaryotic input⁹⁴. Thus, the analysis of Yungay clay-rich soils suggests that the distribution of *n*-alkanes and other biosignatures also reflect a mixed contribution from different types of microorganisms including cyanobacteria that inhabited surface halite and exogenous eukaryotic material. These results highlight the ability of smectite to preserve different types/sources of biosignatures in an environment as extreme as the hyperarid core of the Atacama, with direct implications for the preservation and discovery of biosignatures on Mars⁹⁵.

Finally, we compared the analytical capabilities of the Gas Chromatography-Mass Spectrometry (GC-MS) techniques used on the Yungay clay minerals with the analytical instruments on the Mars rovers *Curiosity*, *Rosalind Franklin*, and *Perseverance*. The Sample Analysis at Mars (SAM) instrument suite on *Curiosity* can detect a wide range of biosignatures, including volatile organics, polar and non-polar organics, complex organics (> 20 C atoms/molecule) and refractory organics⁹⁶. SAM is a suite of three instruments that analyze volatiles released from rock or soil samples using three experimental methods: (1) evolved gas analysis-quadrupole mass spectrometry (EGA-QMS), in which samples are heated to ~ 800 °C and evolved gases are measured by QMS and GC-MS; (2) combustion, in which samples are heated in the presence of O₂ and the products are measured by QMS, GC-MS and/or tunable laser spectrometry (TLS); and (3) wet chemistry experiments, in which samples are derivatized at lower temperatures (up to ~ 300 °C)^{24,96}. Onboard the *Rosalind Franklin* rover, biomarkers may be detected with a mass spectrometer, the Mars Organic Molecule Analyzer (MOMA), and a Raman spectrometer. MOMA is able to operate in two modes: pyrolysis/gas chromatography mass spectrometry (pyr/GC-MS) or laser desorption/ionization mass spectrometry (LDI-MS) at ambient Mars pressures^{97,98}. The Mars2020 *Perseverance* rover, on the other hand, will carry a UV Raman spectrometer, the Scanning Habitable Environments with Raman and Luminescence for Organics and Chemicals (SHERLOC), using fine-scale imaging and a UV laser for the search of biomarkers⁹⁹. Lipid biomarkers (alkanes, isoprenoids, fatty acids or alcohol series) detected with GC-MS techniques in Yungay clay-rich samples and relevant to the search for (a priori prokaryotic) Martian life, are in principle identifiable with the SAM, MOMA and SHERLOC instruments. In fact, lipid detection by SHERLOC should be used as a criterion for sample collection by *Perseverance*. Of the four fundamental biomolecules (lipids, nucleic acids, proteins, and carbohydrates), lipids have the greatest preservation potential over geologic time¹⁰⁰. Carbonaceous chondrites could have carried abiogenic organic compounds to the Martian surface¹⁰¹, which can complicate the detection of biomarkers on Mars. The detection of an even-over-odd preference for fatty acid methyl esters (FAMES, the building blocks of lipids), however, would be a strong indicator of biological processes^{101,102}, assuming Martian biochemistry functions the same as terrestrial biochemistry. Still, key questions arise concerning relevant aspects such as matrix effects or limits of detection. For the GC-MS technique used in this study, samples require specific pre-treatment after organic solvent extraction and prior to analysis, such as separation of the total lipid extract into different polarity fractions (e.g., acidic, apolar and polar) or derivatization with trans-esterification (e.g., BF₃) and tri-methylsilylation (e.g., BSTFA) reagents to convert the acidic and alcohol moieties into GC-MS amenable (i.e., volatile enough) compounds (FAMES and trimethylsilyl ethers, respectively). SAM can perform wet chemistry experiments with tetramethylammonium hydroxide (TMAH) to make lipids sufficiently volatile to detect with GC-MS¹⁰³ and with N-methyl-N-(tert-butyl)dimethylsilyl trifluoroacetamide (MTBSTFA) to detect amino and carboxylic acids⁹⁶. In fact, the first wet chemistry experiment was recently performed on active eolian Martian sand and results are being interpreted¹⁰⁴. *Curiosity* is currently in the smectite-rich Glen Torridon unit, and SAM will perform wet chemistry experiments on a smectite-rich sample to search for complex organics¹⁰⁴. In contrast, analyses with the MOMA and SHERLOC instruments will not involve such a complex pre-treatment. MOMA has the possibility of a derivatization step prior to GC-MS analysis, however, the lack of a previous fractionation step would affect the sample as a whole, not as polarity-specific moieties. As a spectroscopy technique, SHERLOC does not require any derivatization; however, based on fluorescence criteria, it is a technique susceptible to matrix effects that could complicate the detection of organics. Instrument sensitivity is also a key criterion for biomarker detection. SAM has a detection limit similar to the GC-MS technique used to analyze Yungay clay-rich samples (1 ppb or ng g⁻¹). The detection limits for both the MOMA (1 nmol, which could vary between 100–600 ng depending on the molecular weight of the analyzed molecule)^{97,98} and SHERLOC (in the range of ppm) instruments⁹⁹, however, are orders of magnitude greater than SAM. Thus, SAM wet chemistry experiments in the smectite-rich Glen Torridon unit may be our best opportunity to identify biomarkers on Mars prior to sample return. The amount, concentration and distribution of target biomarkers (ppb or ppm) are critical for the success of the two near-future life-detection Martian missions.

A final point to consider for the detection of ancient Martian biomarkers is the alteration of organic molecules over time. The alteration and degradation of organic matter on Earth from burial diagenesis and thermal processes as they relate to hydrocarbon production have been well-studied for decades. Organic matter decomposes during early burial diagenesis typically via oxidation to CO₂ by microorganisms¹⁰⁵. With progressive burial, heat and metamorphism, organic matter is first carbonized, removing most noncarbon elements and forming an aromatic skeleton, then graphitized through polymerization and structural rearrangement of the aromatic skeleton¹⁰⁶. The oldest known sedimentary sequences on Earth (> 3.7 Gyr old) have been metamorphosed such that organic carbon has been graphitized, and whether the graphitized carbon represents traces of early life has been debated^{107,108}. Mars, unlike Earth, never had robust plate tectonics¹⁰⁹ and, as a result, 3–4 Gyr old sedimentary rocks on the Martian surface have, for the most part, been minimally altered since their deposition. Even the ancient smectite-bearing mudstone in Gale crater lacks substantial mineralogical evidence for widespread burial diagenesis (i.e., there is no evidence for illitization)¹¹⁰ despite a potential burial depth of up to 5 km¹¹¹. Therefore, ancient smectite-bearing martian surfaces are ideal locations to investigate habitability in our early Solar System. Ancient sedimentary rocks on Mars have experienced some degree of diagenesis because they are

lithified, cemented and contain mineralized veins and concretions^{112–114}. Diagenesis, in some cases, might work in favor of preserving organic matter on Mars. Thiophenic, aromatic and aliphatic compounds discovered by SAM in Gale crater have sulfur in their structures, suggesting early diagenesis in the presence of reduced sulfur made these molecules recalcitrant²⁵. If sulfurization was a widespread process on early Mars, ancient organic molecules may have been preserved across the planet and may be indeed present in Jezero crater and Oxia Planum. Cosmic radiation on the Martian surface would also have a significant effect on biomarkers, especially those in the top 1 m of the surface¹¹⁵. Radiation oxidizes hydrocarbons and aromatic macromolecules to organic salts and CO₂. The detection of organic molecules by SAM in multiple locations in Gale crater and the presence of organic molecules in carbonaceous chondrites, however, indicates that organic matter can survive long-term exposure to ionizing radiation¹¹⁵.

Conclusions

The results presented here, showing that wet subsurface clay minerals are inhabited by a number of metabolically active microorganisms in the midst of the driest place on earth, isolated and protected just centimeters below the extremely harsh surface environmental conditions typical of the Atacama, reinforce the notion that early Mars could have been a planet with similar subsurface protected habitable niches, particularly during the first billion years of its history. Orbital and *in-situ* measurements demonstrate a heterogeneous distribution of smectite and other clay minerals in Noachian- and early Hesperian-aged (~ 3.5 Gyr ago) surfaces^{116,117}. Computer simulations and geochemical models suggest that clay minerals could have formed during relatively short warmer and wetter cycles in a predominantly dry and/or cold early Mars^{118,119}. Thus, much of early Mars' history may have been similar to the modern Atacama, where wetting events were very rare. Because of colder conditions on early Mars, liquid water may have been generated by melting ice, rather than rain.

The known patchy distribution of subsurface habitats in the hyperarid core of the Atacama^{29,120,121} suggests that the search for biosignatures on Mars with the scientific payloads of future rovers will be a difficult task, as potential biosignatures could be similarly unevenly distributed throughout the Martian subsurface. Because the subsurface microbial community discovered in Yungay has adapted to an environment of persistent superficial drought with rare exposure to water, this expands potentially habitable environments on Mars to those with evidence for sporadic exposure to water, rather than persistent exposure. Fracture-associated halos in Gale crater, for example, extend into clay-rich rocks and represent locations where multiple fluid episodes altered the rock^{122,123}. These clay-rich, subsurface zones may have been habitable to microorganisms similar to those found in subsurface soils in Yungay. If similar zones of aqueous alteration along fractures are discovered in Jezero crater, we suggest these should be high-priority targets for sample selection with *Perseverance* for eventual return to Earth. Our results also have implications for planetary protection constraints¹²⁴, as ExoMars has a 2 m drill that could easily reach undetected, potentially inhabited clay minerals below the Martian surface. Ancient, smectite-bearing rocks, however, may not be as habitable as unlithified soils because there may not be sufficient pore space for microorganisms to inhabit and the structural water in smectite-bearing rock may not be as readily available to microorganisms. The findings reported here may be considered as a guide to the search for hotspots preserving molecular biomarkers, and potentially life, well-protected below the Martian surface.

Materials and methods

Sampling sites and dates. Twenty soil samples were first taken in the field on 13 March 2017 using sterile gloves and sterile falcon tubes (Thermo Fisher Scientific, Massachusetts, USA), on a pit dug in the region of Yungay with coordinates 24°5'4.52"S, 69°54'55.11"W. Twenty additional samples were taken from this pit on 8 March 2018. Four other pits were dug on 20 August 2018, with coordinates 24°4'57.9"S, 69°54'55.50"W; 24°5'24.70"S, 69°54'40.50"W; 24°4'37.9"S, 69°54'48.50"W and 24°4'19.46"S, 69°53'58.86"W. Pits were dug to a depth of ~ 70 cm. All samples were stored inside a plastic cooler at room temperature at all times from the sampling site to the lab.

Light penetration in the soil. Light penetration in the soil was measured in the field with a digital lux meter (Bestone Industrial Co., Ltd., Shenzhen, China). Measurements were taken by leaving the digital lux meter at the soil surface for 1 min, and then burying the sensor portion of the digital lux meter at one, and three centimeters of depth for the same amount of time.

Environmental characterization (temperature and relative humidity). Temperature and relative humidity were measured in the field using dual iButton temperature/Humidity micro loggers (Maxim Integrated, San Jose, CA, USA) as previously done⁴⁶, set to take data every 10 min during 28 July and 19 August 2018, and every 5 min between 22 and 29 July 2019. These sensors were set at the soil surface (shaded under a small rock) and also completely buried at 20 and 40 cm depth, with the sensor set at 40 cm well-immersed in the wet clay-rich soil. Environmental data statistical analyses: Pearson correlation coefficient. The number of degrees of freedom for *r* is *n*-2, where *n* is the number of pairs of bivariate data, for this case 782 for each correlation. Level of significance: alpha = 0.05.

X-ray diffraction. Bulk samples were stored at room temperature and then ground in the lab into powder with an agate mortar and pestle (Pulverisette 2, Fritsch, Idar-Oberstein, Germany), and X-ray powder diffraction data were collected using a Bruker D8 Eco Advance (Massachusetts, USA) in Bragg–Brentano geometry, Cu K α radiation and Lynxeye XE-T linear detector. The X-ray generator was operated at 40 kV and 25 mA. Samples were scanned with a 0.05° (2 θ) step size, over the range 5–60° (2 θ) with a 1 s collection time at each step. Phase identification was performed by comparing the measured diffraction pattern (diffractograms) with patterns of

the PDF Database with the DIFFRAC.EVA software (Bruker AXS, Massachusetts, USA). Oriented clay mounts were prepared using the filter-peel method¹²⁵.

Clay characterization. Bulk samples in the lab were stored at room temperature and then dispersed in sodium hexametaphosphate (HMP 5%wt). Size fractionation was performed by low-speed centrifugation to obtain a suspension of the < 2 µm size fraction according to Stokes' law (also used for clay percentage determination). The suspension of clay-sized particles was titrated (acetate buffer, pH 5.0, until a pH of 6.8 was obtained) and washed with distilled water to remove carbonates and soluble salts, respectively.

Near-infrared spectroscopy. Near-infrared spectra of the clay-sized separates were stored at room temperature and then analyzed in the lab using the diffuse reflection method¹²⁶ (DRIFT) with a Nicolet FTIR spectrometer (Thermo Fisher Scientific, Massachusetts, USA). Samples were poured into a sample cup without dilution in KBr. Analysis were done at room temperature and under air-dried atmosphere. We used a mirror for background measurement. Spectra were collected using a DTGS-KBr detector at 2 cm⁻¹ resolution in the NIR region (from 12,000 to 4000 cm⁻¹; 1 to 2.5 µm) with a quartz beamsplitter.

Bacterial counts. Microorganisms in clay bearing soils were stored at room temperature and then enumerated by direct counts in the bulk samples in the lab. As cell visualization is less efficient when minerals mask cells by adsorbing traditional dyes, we used SYBR Green I (Molecular Probes, Eugene, USA) instead of DAPI (4',6-Diamidino-2-Phenylindole, Dihydrochloride). Briefly, 2 g of clay samples (incubated for 2 weeks at 37 °C) were suspended in 10 mL of 0.01 M tetrasodium pyrophosphate and gently sonicated in a Branson ultrasonic cleaner (Danbury, USA) for 30 min in ice cooled water. After 10 s of sedimentation, 2 mL of the supernatant were taken and placed directly on black Isopore polycarbonate membrane filter (0.2 µm pore size, Millipore, Massachusetts, USA). Membranes were then incubated with 1.5 mL of SYBR Green I (50 µg/L) during 15 min in the dark. Membranes were then washed with 10 mL of distilled water and left in dark for air drying. One drop of immersion oil was deposited on glass slide, then the filter and another drop of oil was deposited on the filter surface and covered with a glass cover. Bacteria were counted immediately using Zeiss AxioImager M.2 fluorescence microscope (Carl Zeiss, Jena, Germany) and a Plan-Apo 63x/1.4 Zeiss oil-immersion objective. Filter set for eGFP (Zeiss Filter Set 38; Excitation/Emission: 450–490/500–550 nm) was used for SBI stained bacteria visualization. Bacteria were counted by selecting random fields of view, with 20 fields per filter analyzed. Five filters were counted per sample, for a total of 10 filters and 200 fields observed.

DNA extraction from isolates. Clay samples were stored at room temperature and DNA extracted from them in the lab using the DNeasy UltraClean Microbial Kit (Quiagen, Düsseldorf, Germany) according to the manufacturer instruction and as previously performed, except that at the cell lysis step, two pulses of 2 min were used in a FastPrep-24 5G homogenizer (MP Biomedicals, Irvine, USA).

Illumina NGS-based 16S rRNA Sequencing. Illumina sequencing in the lab was performed using the DNA extracted from the clay samples by the Fundación Parque Científico Madrid (FPCM, Madrid, Spain) sequencing service using their standard procedures as follows. Bacterial 16S rRNA V3-V4 hypervariable gene region was amplified with the primer pair 341f. (5'CCTACGGGNGGCWGCAG3') and 805r (5'GACTAC HVGGGTATCTAATCC')¹²⁷. After DNA extraction from soil samples, PCR and Illumina MiSeq (Berlin, Germany), sequencing were carried out at the Genomic Service of FPCM.

Purified DNAs were amplified in a first PCR of 30 cycles with Q5 Hot Start High-Fidelity DNA Polymerase (New England Biolabs, Massachusetts, USA) in the presence of 100 nM primers S-D-Bact-0341-b-S-17 (5'-ACA CTGACGACATGGTTCTACACCTACGGGNGGCWGCAG-3' and S-D-Bact-0785-a-A-21 5'-TACGGTAGC AGAGACTTGGTCTGACTACHVGGGTATCTAATCC-3'), for the amplification of the V3-V4 region of 16S rRNA. After the first PCR, a second PCR of 15 cycles was performed with Q5 Hot Start High-Fidelity DNA Polymerase (New England Biolabs, Massachusetts, USA) in the presence of 400 nM of primers 4242A1 (5'-AAT GATACGGCGACCAACCGAGATCTCACTGACGACATGGTTCTACA-3' and 806R 5'-CAAGCAGAAGAC GGCATACGAGAT-(10 nucleotides barcode)-534R TACGGTAGCAGAGACTTGGTCT-3') of the Access Array Barcode Library for Illumina Sequencers (Fluidigm, San Francisco, USA). The finally obtained amplicons were validated and quantified by Bioanalyzer and an equimolecular pool was purified using AMPure beads (Beckman Coulter, Pasadena, USA) and titrated by quantitative PCR using the Kapa-SYBR FAST qPCR kit for LightCycler480 (Kapa Biosystems, Cape Town, South Africa) and a reference standard for quantification. The pool of amplicons was denatured prior to be seeded on a flowcell at a density of 10 pM, where clusters were formed and sequenced using a MiSeq Reagent Nano Kit v2 (Illumina, Berlin, Germany) in a 2 × 250 pair-end sequencing run on a MiSeq sequencer (Illumina, Berlin, Germany).

Raw sequences were processed in MOTHUR software v.1.40.5¹²⁸, using a custom script based on MiSeq SOP¹²⁹. Briefly, reads below 400 bp, with ambiguous nucleotide identities and/or homopolymers longer than 8 bp, singletons and putative chimeras were removed from subsequent analyses. Remaining reads were then clustered into OTUs (Operational Taxonomic Units) at the 97% similarity level. Number of sequences were finally normalized among samples to the lesser number of reads, i.e. 9823, by random selection. Taxonomic assignments were performed by comparing OTU's representative sequences with RDP database¹³⁰, as it is the most up-to-date database that can be included in MOTHUR analyses, as well as the most accurate in assigning real taxonomic affiliation of OTUs obtained from desert samples⁷⁹. OTUs assigned to 'cyanobacteria/chloroplast' were further compared with NCBI GenBank, EMBL, Greengenes and SILVA databases for more precise cyanobacteria taxonomic identification.

Cultivation of isolates from clay samples. In the lab, clay samples were stored at room temperature and then aseptically inoculated in Petri dishes containing agar and either Luria–Bertani Broth (Sigma–Aldrich, Missouri, USA) or Marine Media (CondaLab, Torrejón de Ardoz, Spain). Colonies arising from clay particles usually were evident 2–3 days after inoculation. These colonies were then re-cultivated in the media from they were first isolated to obtain enough biomass for DNA extraction and storage. *Lysinibacillus* and *Oceanobacillus* species were able to grow both in Luria–Bertani Broth and Marine Media agar plates, while all other species were able to grow only in Luria–Bertani Broth agar plates. The a_w measured inside sealed Petri dishes containing Luria–Bertani Broth agar was 0.985, while the a_w measured inside sealed Petri dishes containing Marine Media agar plates was 0.973.

16S rRNA amplification and sequencing from isolates DNA. As previously performed⁶⁹, 16S rRNA of bacterial isolates was amplified in the lab using the GoTaq Green Master Mix (Promega, Wisconsin, USA) and the primers 341f. (5'CCTACGGGNGGCWGCAG3') and 785r (5'GACTACHVGGGTATCTAATCC'). PCR conditions used were: 95 °C for 5 min, and 25 cycles of (95 °C for 40 s, 55C for 2 min, 72 °C for 1 min) followed by 72 °C for 7 min. The resultant reactions were visualized in a 2% agarose TAE gel at 50 V.

The automated sequencing of the resulting PCR products was conducted by MacroGen DNA Sequencing Inc. (Seoul, Korea). Sequences were checked for quality using the BioEdit software (Ibis Therapeutics, Carlsbad, USA) and end-trimmed before using the Megablast option for highly similar sequences of the BLASTN algorithm against the National Centre for Biotechnology Information nonredundant database (www.ncbi.nlm.nih.gov) to search for the closest species of each of the isolates obtained. Only species with at least 98% of sequence identity and an E value of 0.0 were selected, and only species with defined genus and species names were considered for phylogenetic closeness.

Phylogenetic analysis. In the lab, phylogenetic analysis of 16S rRNA gene sequences obtained from isolates were aligned by multiple sequence comparison by log-expectation¹³¹, analyzed with jModelTest¹³² and then by Phylip NJ (bootstrap 10,000)¹³³, all tools of the freely available Bosque phylogenetic analysis software (version 1.7.152)¹³⁴.

Fluorescence microscopy, SYBR green and CTC staining. Small fragments of moist clay aggregates from Yungay (about 1 cm³) were carefully cut with a sterile blade in the lab. Plane clay surfaces were stained during 30 min at 37 °C in dark with 100 µL (1:100 dilution) of SYBR Green I (SBI) (Molecular Probes, Eugene, USA), a fluorochrome specific for staining nucleic acids. Multichannel Image Acquisition (MIA) system was used with combination of following filter sets: filter set for eGFP (Zeiss Filter Set 38; Ex/Em: 450–490/500–550 nm) and Rhodamine (Zeiss Filter Set 20; Ex/Em: 540–552/567–647 nm) and autofluorescence signal potentially proceeded from extracellular polymeric substances (EPS), respectively. The eGFP and DAPI (Zeiss Filter Set 49; Ex/Em: 365/420–470 nm) filter sets were used for acquisition of single section images of SBI stained nucleic acids and autofluorescence signal potentially proceeded from EPS, respectively. Likewise, plane clay surfaces were stained during 24 h at 25 °C in dark with 100 µL of 5 mM of tetrazolium salt: 5-cyano-2,3-ditolyl tetrazolium chloride (CTC) (Molecular Probes, Eugene, USA)¹³⁵. The formazan crystals are viewed as yellow-orange fluorescent spots when using Ex/Em: 426–446/545–645 nm filter set.

After both stains, a drop of immersion oil was placed on plane clay surfaces. After covering a clay surface with a square coverslip the samples were visualized with Zeiss AxioImager M.2 fluorescence microscope (Carl Zeiss, Jena, Germany) and a Plan-Apo 60x/1.4 Zeiss oil-immersion objective. In some cases for better 3D visualization of bacteria aggregates, the Maximum Image Projection (MIP) images were reconstructed using the software package AxioVision 4.8.1 (Carl Zeiss, Jena, Germany).

EPS are a complex mixture of biomolecules; polysaccharides, proteins, nucleic acids, lipids and other macromolecules. Proteins and exopolysaccharides represent the key components of EPS, accounting for 40–95% of its structure. There are at least two components of EPS which can produce a signal in fluorescence microscopy; proteins and nucleic acids. We used SYBR Green staining for staining bacterial nucleic acids, thus disperse nucleic acids in the EPS should also be stained, leading to a detectable, although weaker, signal in FM. Some clays can produce a very weak autofluorescence signal, however, we did not observe any clay autofluorescence, but only the autofluorescence of proteins and the fluorescence coming from the SYBR Green stained nucleic acids.

Biosignature analyses. Biosignatures analysis were performed as previously reported by us¹³⁶.

A. Geolipid extraction, fractionation and analysis

Sediment sample (~ 50 g) was extracted with a mixture of dichloromethane/methanol (DCM/MeOH, 3:1, v/v) for 24 h with a Soxhlet apparatus (Fisher Scientific, New Hampshire, USA). Internal standards (tetracosane-D50, myristic acid-D27, 2-hexadecanol) were added prior to extraction. The total lipid extracts were concentrated by rotary evaporation to 2 ml. After this step, activated copper was added and allowed to stand overnight to remove elemental sulfur. The extracted sample was separated in two fractions using a Bond-elute column chromatography (bond phase NH₂, 500 mg, 40 µm particle size). The neutral lipid fraction was obtained by eluting with 15 ml DCM/2-propanol (2:1, v/v) and the acid fraction with 15 ml of acetic acid (2%) in diethyl ether. Further separation of the neutral lipid fraction was done with 0.5 g of alumina in a Pasteur pipet. The non-polar fraction was obtained by eluting 4.5 ml of hexane/DCM (9:1, v/v) and the polar fraction with 3 ml of DCM/methanol (1:1, v/v). The acid fraction was derivatized with BF₃ in methanol and the polar fraction with N,O-bis (trimethylsilyl) trifluoroacetamide (BSTFA).

B. Gas chromatography-mass spectrometry (GC–MS) analysis

The sample (non-polar, acid, and polar fraction) was analyzed by gas chromatography mass spectrometry using a 6850 GC system coupled to a 5975 VL MSD with a triple axis detector (Agilent Technologies, Santa Clara, USA) operating with electron ionization at 70 eV and scanning from 50 to 650 m/z. The analytes were injected (1 μ l) and separated on a HP-5MS column (30 m \times 0.25 mm i.d. \times 0.25 μ m film thickness) using He as a carrier gas at 1.1 ml min⁻¹. For the non-polar fraction, the oven temperature was programmed from 50 to 130 °C at 20 °C min⁻¹ and then to 300 °C at 6 °C min⁻¹ (held 20 min). For the acid fraction the oven temperature was programmed from 70 to 130 °C at 20 °C min⁻¹ and then to 300 °C at 10 °C min⁻¹ (held 10 min). For the polar fraction the oven temperature program was the same as that for the acid fraction, but the oven was held for 15 min at 300 °C. The injector temperature was 290 °C, the transfer line was 300 °C, and the MS source was 240 °C. Compound identification was based on the comparison of mass spectra and/or reference compounds, compounds were quantified with external calibration curves. External standards of *n*-alkanes (C10 to C40), fatty acids methyl esters, FAMES (C8 to C24), alkanols (C10, C14, C18, C20), and branched isoprenoids (2,6,10-trimethyl-docosane, crocetane, pristane, phytane, squalane and squalene) were injected to obtain calibration curves. Recoveries of the internal standards averaged 69 \pm 18%.

C. Stable isotopes analysis: organic carbon and total nitrogen

Total nitrogen ($\delta^{15}\text{N}$) and organic carbon ($\delta^{13}\text{C}$) isotopes were measured by USGS methods¹³⁷. Briefly, sediment sample (2 g) was homogenized by grinding with a corundum mortar and pestle. Then HCl was added to 0.5 g of sample to remove carbonate, equilibrated for 24 h, and adjusted to neutral pH with ultrapure water, dried at oven (50 °C), and analyzed in the IRMS (MAT 253, Thermo Fisher Scientific, Massachusetts, USA). $\delta^{13}\text{C}$ and $\delta^{15}\text{N}$ values were reported in the standard per mil notation using three certified standards (USGS41, IAEA-600, and USGS40), analytical precision of 0.1‰.

D. Compound specific isotope analysis

Conditions for gas chromatography analysis of isotopic ratio of *n*-alkanes, were identical with standard GC–MS analysis for the polar fraction. Carbon isotopic composition of individual compounds were performed using an isotope ratio gas-chromatograph–mass spectrometry (GC-IRMS) system, a Trace GC 1310 ultra, coupled to a MAT 253 IRMS (Thermo Fisher Scientific, Massachusetts, USA). Conditions in the IRMS were as follows: electron ionization 100 eV, Faraday cup collectors m/z 44, 45 and 46, a CuO/NiO combustion interface maintained at 1000 °C. The samples were injected in splitless mode (inlet temperature 250 °C, helium as a carrier gas at constant flow of 1.1 ml min⁻¹). The isotopic values of peaks produced in the combustion reactor of the chromatography separated compounds were calculated using CO₂-spikes of known isotopic composition, introduced directly into the source three time at the beginning and at the end of every run. An *n*-alkane reference mixture with known isotopic composition (A6, Indiana University, USA) were run after every four samples to check accuracy of the isotopic ratio determined by the GC-IRMS.

Data availability

Data and materials are available, and should be requested to A.A-B.

Received: 23 June 2020; Accepted: 16 October 2020

Published online: 05 November 2020

References

- Lakdawalla, E. Similarities and differences in the landing sites of ESA's and NASA's 2020 Mars rovers. *Nat. Astron.* **3**, 190–192 (2019).
- Poulet, F. *et al.* Mawrth Vallis, Mars: a fascinating place for future in situ exploration. *Astrobiology* **20**, 1–36 (2019).
- Fassett, C. I. & Head, J. W. Fluvial sedimentary deltas on Mars: ancient deltas in a crater lake in the Nili Fossae region. *Geophys. Res. Lett.* **32**, L14201 (2005).
- Schon, S. C., Head, J. W. & Fassett, C. I. An overfilled lacustrine system and progradational delta in Jezero Crater, Mars: implications for noachian climate. *Planet. Space Sci.* **67**, 28–45 (2012).
- Goudge, T. A., Mohrig, D., Cardenas, B. T., Hughes, C. M. & Fassett, C. I. Stratigraphy and paleohydrology of delta channel deposits, Jezero crater, Mars. *Icarus* **301**, 58–75 (2018).
- Horgan, B. H. N., Anderson, R. B., Dromart, G., Amador, E. S. & Rice, M. S. The mineral diversity of Jezero crater: evidence for possible lacustrine carbonates on Mars. *Icarus* **339**, 113526 (2020).
- Ehlmann, B. L. *et al.* Identification of hydrated silicate minerals on Mars using MRO-CRISM: geologic context near Nili Fossae and implications for aqueous alteration. *J. Geophys. Res.: Planets* **114**, E00D08 (2009).
- Mustard, J. F. *et al.* Hydrated silicate minerals on Mars observed by the Mars reconnaissance orbiter CRISM instrument. *Nature* **454**, 395–309 (2008).
- Goudge, T. A., Mustard, J. F., Head, J. W., Fassett, C. I. & Wiseman, S. M. Assessing the mineralogy of the watershed and fan deposits of the Jezero crater paleolake system, Mars. *J. Geophys. Res.: Planets* **120**, 775–808 (2015).
- Borchardt, G. Smectites. *Miner. Soil Environ.* **1**, 675–727 (1989).
- Vago, J. L. *et al.* Habitability on early Mars and the search for biosignatures with the exomars rover. *Astrobiology* **17**, 471–510 (2017).
- Quantin-Nataf, C. *et al.* Oxia Planum, the landing site for ExoMars 2018. In *47th Lunar and planetary science conference abstracts* 2863 (2016).
- Quantin-Nataf, C., Thollot, P., Carter, J., Mandon, L. & Dehouck, E. The unique and diverse record of noachian aqueous activity in Oxia Planum, Mars. *Lunar and Planetary Science Conference* **2018**, 2083 (2018).
- Milliken, R. E., Grotzinger, J. P. & Thomson, B. J. Paleoclimate of Mars as captured by the stratigraphic record in Gale Crater. *Geophys. Res. Lett.* **37**, L04201 (2010).
- Wray, J. J. Gale crater: the Mars science laboratory/curiosity rover landing site. *Int. J. Astrobiol.* **12**, 25–38 (2013).
- Ehlmann, B. L. *et al.* Clay minerals in delta deposits and organic preservation potential on Mars. *Nat. Geosci.* **1**, 355–358 (2008).
- Hoehler, T. An energy balance concept for habitability. *Astrobiology* **7**, 824–838 (2007).

18. Summons, R. E. *et al.* Preservation of Martian organic and environmental records: final report of the mars biosignature working group. *Astrobiology* **11**, 157–181 (2011).
19. Bibring, J. P. *et al.* Global mineralogical and aqueous Mars history derived from OMEGA/mars express data. *Science* **312**, 400–404 (2006).
20. Grotzinger, J. P. *et al.* A habitable fluvio-lacustrine environment at Yellowknife Bay, Gale crate, Mars. *Science* **343**, 1242777 (2014).
21. Kennedy, M. J., Pevear, D. & Hill, R. Mineral surface control of organic carbon in black shale. *Science* **295**, 657–660 (2002).
22. Theng, B. K. G., Churchman, G. J. & Newman, R. H. The occurrence of interlayer clay-organic complexes in two New Zealand soils. *Soil Sci.* **142**, 262–266 (1986).
23. Wattel-Koekkoek, E. J. W., van Genuchten, P. P. L., Buurman, P. & van Lagen, B. Amount and composition of clay-associated soil organic matter in a range of kaolinitic and smectitic soils. *Geoderma* **99**, 27–49 (2001).
24. Freissinet, C. *et al.* Organic molecules in the Sheepbed Mudstone, Gale Crater, Mars. *J. Geophys. Res.: Planets* **120**, 495–514 (2015).
25. Eigenbrode, J. L. *et al.* Organic matter preserved in 3-billion-year-old mudstones at Gale crater, Mars. *Science* **360**, 1096–1110 (2018).
26. Vago, J. *et al.* ESA ExoMars program: the next step in exploring Mars. *Sol. Syst. Res.* **49**, 518–528 (2015).
27. Navarro-Gonzalez, R. *et al.* Mars-like soils in the Atacama Desert, Chile, and the dry limit of microbial life. *Science* **302**, 1018–1021 (2003).
28. McKay, C. P. *et al.* Temperature and moisture conditions for life in the extreme arid region of the Atacama Desert: four years of observations including the El Nino of 1997–1998. *Astrobiology* **3**, 393–406 (2003).
29. Sutter, B., Dalton, J. B., Ewing, S. A., Amundson, R. & McKay, C.P. Terrestrial analogs for interpretation of infrared spectra from the Martian Surface and subsurface: sulfate, nitrate, carbonate, and phyllosilicate-bearing Atacama Desert soils. *J. Geophys. Res.* **112**, G04S10. <https://doi.org/10.1029/2006JG000313> (2007).
30. Ewing, S. A., Macalady, J. L., Warren-Rhodes, K., McKay, C. P. & Amundson, R. Changes in the soil C cycle at the arid-hyperarid transition in the Atacama Desert. *J. Geophys. Res.* **113**, G02S90. <https://doi.org/10.1029/2007JG000495> (2008).
31. Wilhelm, M. B. *et al.* Xeropreservation of functionalized lipid biomarkers in hyperarid soils in the Atacama Desert. *Org. Geochem.* **103**, 97–104 (2017).
32. Azua-Bustos, A., Caro-Lara, L. & Vicuña, R. Discovery and microbial content of the driest site of the hyperarid Atacama Desert, Chile. *Environ. Microbiol. Rep.* **7**, 388–394 (2015).
33. Fletcher, L. E. *et al.* Determination of low bacterial concentrations in hyperarid Atacama soils: comparison of biochemical and microscopy methods with real-time quantitative PCR. *Can. J. Microbiol.* **57**, 953–996 (2011).
34. Azua-Bustos, A., Urrejula, C. & Vicuña, R. Life at the dry edge: microorganisms of the Atacama Desert. *FEBS Lett.* **586**, 2939–2945 (2012).
35. Cordero, R. R. *et al.* Ultraviolet radiation in the Atacama Desert. *Antonie Van Leeuwenhoek* **111**, 1301–1313 (2018).
36. Ewing, S. A. *et al.* A threshold in soil formation at Earth's arid-hyperarid transition. *Geochim. Cosmochim. Acta* **70**, 5293–5322 (2006).
37. Ewing, S.A. *et al.* Rainfall limit of the N cycle on earth. *Global Biogeochem. Cycles* **21**, GB3009 (2007).
38. Robinson, C. K. *et al.* Microbial diversity and the presence of algae in halite endolithic communities are correlated to atmospheric moisture in the hyper-arid zone of the Atacama Desert. *Environ. Microbiol.* **17**, 299–315 (2014).
39. Wierzchos, J. *et al.* Microbial colonization of Ca-sulfate crusts in the hyperarid core of the Atacama Desert: implications for the search for life on Mars. *Geobiology* **9**, 44–60 (2010).
40. Wierzchos, J., Ascaso, C. & McKay, C. P. Endolithic cyanobacteria in Halite rocks from the hyperarid core of the Atacama Desert. *Astrobiology* **6**, 415–422 (2006).
41. Wang, F., Michalski, G., Seo, J. & Ge, W. Geochemical, isotopic, and mineralogical constraints on atmospheric deposition in the hyper-arid Atacama Desert, Chile. *Geochim. Cosmochim. Acta* **135**, 29–48 (2014).
42. Wierzchos, J., de los Ríos, A. & Ascaso, C. Microorganisms in desert rocks: the edge of life on earth. *Int. Microbiol.* **5**, 172–182 (2012).
43. Skoog, A. D., West, D. M., Holler, F. J., Stanley, R. & Crouch, S. R. *Fundamentals of analytical chemistry* 9th edn. (Cengage Learning, Brooks/Cole, 2013).
44. Huat, B. B. K., Toll, D. G. & Prasad, A. *Handbook of tropical residual soils engineering* 1st edn. (CRC Press, Boca Raton, 2017).
45. Jordan, T. E. *et al.* Isotopic characteristics and paleoclimate implications of the extreme precipitation event of March 2015. *Andean Geol.* **46**, 1–31 (2019).
46. Azua-Bustos, A. *et al.* Unprecedented rains decimate surface microbial communities in the hyperarid core of the Atacama Desert. *Nat. Sci. Rep.* **8**, 16706 (2018).
47. Osterloo, M. M. *et al.* Geologic context of proposed chloride-bearing materials on Mars. *J. Geophys. Res.: Planets* <https://doi.org/10.1029/2010JE003613> (2010).
48. Rapin, W. *et al.* An interval of high salinity in ancient Gale crater lake on Mars. *Nat. Geosci.* **12**, 889–895 (2019).
49. Murchie, S. L. *et al.* A synthesis of Martian aqueous mineralogy after 1 Mars year of observations from the Mars Zzzbiter. *J. Geophys. Res.: Planets* <https://doi.org/10.1029/2009JE003342> (2009).
50. Milliken, R. E. *et al.* Paleoclimate of Mars as captured by the stratigraphic record in Gale crater. *Geophys. Res. Lett.* <https://doi.org/10.1029/2009GL041870> (2010).
51. Palucis, M. C. *et al.* Sequence and relative timing of large lakes in Gale crater (Mars) after the formation of Mount Sharp. *J. Geophys. Res.: Planets* **121**(3), 472–496 (2016).
52. Vitek, P. *et al.* Microbial colonization of halite from the hyper-arid Atacama Desert studied by Raman spectroscopy. *Philos. Trans. R. Soc. A Math. Phys. Eng. Sci.* **368**, 3205–3221 (2010).
53. Flemming, H. C. *et al.* Biofilms: an emergent form of bacterial life. *Nat. Rev. Microbiol.* **14**, 563–575 (2016).
54. Schulze-Makuch, D. *et al.* Transitory microbial habitat in the hyperarid Atacama Desert. *Proc. Natl. Acad. Sci. U.S.A.* **115**, 2670–2675 (2018).
55. Lester, E. D., Satomi, M. & Ponce, A. Microflora of extreme arid Atacama Desert soils. *Soil Biol. Biochem.* **39**, 704–708 (2007).
56. de los Ríos, A. *et al.* Comparative analysis of the microbial communities inhabiting halite evaporites of the Atacama Desert. *Int. Microbiol.* **13**, 78–89 (2010).
57. Orlando, J., Carú, M., Pommerenke, B. & Braker, G. Diversity and activity of denitrifiers of Chilean arid soil ecosystems. *Front. Microbiol.* **3**, 101 (2012).
58. Neilson, J. W. *et al.* Life at the hyperarid margin: novel bacterial diversity in arid soils of the Atacama Desert, Chile. *Extremophiles* **16**, 553–566 (2012).
59. Warren-Rhodes, K. A. *et al.* Cyanobacterial ecology across environmental gradients and spatial scales in China's hot and cold deserts. *FEMS Microbiol. Ecol.* **61**, 470–482 (2007).
60. Parro, V. *et al.* A Microbial oasis in the hypersaline atacama subsurface discovered by a life detector chip: implications for the search for life on Mars. *Astrobiology* **11**, 969–996 (2011).
61. Campos, V. L., León, C., Mondaca, M. A., Yañez, J. & Zaror, C. Arsenic mobilization by epilithic bacterial communities associated with volcanic rocks from Camarones River, Atacama Desert, Northern Chile. *Arch. Environ. Contam. Toxicol.* **61**, 185–192 (2010).

62. Crits-Christoph, A. *et al.* Functional interactions of archaea, bacteria and viruses in a hypersaline endolithic community. *Environ. Microbiol.* **18**, 2064–2077 (2016).
63. Bagaley, D. Uncovering bacterial diversity on and below the surface of a hyper-arid environment, the Atacama Desert, Chile. *LSU Masters thesis* 3474 (2006).
64. Moreno, M. L. *et al.* Analysis and characterization of cultivable extremophilic hydrolytic bacterial community in heavy-metal-contaminated soils from the Atacama Desert and their biotechnological potentials. *J. Appl. Microbiol.* **113**, 550–559 (2012).
65. Piubeli, F. *et al.* Phylogenetic profiling and diversity of bacterial communities in the Death valley, an extreme habitat in the Atacama Desert. *Indian J. Microbiol.* **55**, 392–399 (2015).
66. Thomas, D. J. *et al.* Extremophiles for eco-poleis: desirable traits for and survivability of pioneer Martian organisms. *Gravitat. Space Biol.* **19**, 91–104 (2006).
67. Kuhlman, K. R., Venkat, P., La Duc, M. T., Kuhlman, G. M. & McKay, C. P. Evidence of a microbial community associated with rock varnish at Yungay, Atacama Desert. *Chile. J. Geophys. Res. Biogeosci.* **113**, 22 (2008).
68. Paulino-Lima, I. G. *et al.* Isolation of UVC-tolerant bacteria from the hyperarid Atacama Desert, Chile. *Microb. Ecol.* **65**, 325–335 (2012).
69. Azua-Bustos, A. *et al.* Aeolian transport of viable microbial life across the Atacama Desert, Chile: implications for Mars. *Sci. Rep.* **9**, 1–11 (2019).
70. Wilhelm, M. B. *et al.* Constraints on the metabolic activity of microorganisms in Atacama surface soils inferred from refractory biomarkers: implications for Martian habitability and biomarker detection. *Astrobiology* **18**, 955–966 (2018).
71. Roldán, M., Ascaso, C. & Wierzchos, J. Fluorescent fingerprints of endolithic phototrophic cyanobacteria living within Halite rocks in the Atacama Desert. *Appl. Environ. Microbiol.* **80**, 2998–3006 (2014).
72. Langworthy, T. A., Holzer, G., Zeikus, J. G. & Tornabene, T. G. Iso- and anteiso-branched glycerol diethers of the thermophilic anaerobe *Thermodesulfotobacterium commune*. *Syst. Appl. Microbiol.* **4**, 1–17 (1983).
73. Jahnke, L. L. *et al.* Signature lipids and stable carbon isotope analyses of octopus spring hyperthermophilic communities compared with those of aquificales representatives. *Appl. Environ. Microbiol.* **67**, 5179–5189 (2001).
74. Rontani, J. F. & Volkman, J. K. Lipid characterization of coastal hypersaline cyanobacterial mats from the Camargue (France). *Org. Geochem.* **36**, 251–272 (2005).
75. Pagès, A. *et al.* Lipid biomarker and isotopic study of community distribution and biomarker preservation in a laminated microbial mat from Shark Bay, Western Australia. *Microb. Ecol.* **70**, 459–472 (2015).
76. Zhang, C. L. *et al.* Lipid biomarkers, carbon isotopes, and phylogenetic characterization of bacteria in California and Nevada hot springs. *Geomicrobiol. J.* **24**, 519–534 (2007).
77. Meyers, P. A. & Ishiwatari, R. Lacustrine organic geochemistry—an overview of indicators of organic matter sources and diagenesis in lake sediments. *Org. Geochem.* **20**, 867–900 (1993).
78. Volkman, J. K. *et al.* Microalgal biomarkers: a review of recent research developments. *Org. Geochem.* **29**, 1163–1179 (1998).
79. Dembitsky, V. M., Dor, I., Shkrob, I. & Aki, M. Branched alkanes and other apolar compounds produced by the cyanobacterium *microcoleus vaginatus* from the Negev Desert. *Russ. J. Bioorg. Chem.* **27**, 110–119 (2001).
80. Sánchez-García, L. *et al.* Molecular biomarkers in the subsurface of the Salar Grande (Atacama, Chile) evaporitic deposits. *Biogeochemistry* **140**, 31–52 (2018).
81. Shiea, J., Brassel, S. C. & Ward, D. M. Comparative analysis of extractable lipids in hot spring microbial mats and their component photosynthetic bacteria. *Org. Geochem.* **17**, 309–319 (1991).
82. Goosens, H., de Leeuw, J. W., Schenck, P. A. & Brassell, S. C. Tocopherols as likely precursors of pristane in ancient sediments and crude oils. *Nature* **312**, 440–442 (1984).
83. Brocks, J. J. & Summons, R. E. Sedimentary hydrocarbons, biomarkers for early life. In *Biogeochemistry: Treatise on Geochemistry* Vol. 8 (ed. Schlesinger, W. H.) 63–115 (Oxford, Elsevier Pergamon, 2004).
84. Ten Haven, H. L. *et al.* Application of biological markers in the recognition of palaeohypersaline environments. *Geol. Soc. Spec. Publ.* **40**, 123–130 (1988).
85. Carrizo, D., Sánchez-García, L., Rodríguez, N. & Gómez, F. Lipid Biomarker and carbon stable isotope survey on the dallo hydrothermal system in Ethiopia. *Astrobiology* **19**, 1474–1489 (2019).
86. Patterson, G. W. & Nes, W. D. *Physiology and Biochemistry of Sterols* (American Oil Chemists' Society, Champaign, IL, 1991).
87. Goad, L. J. & Akihisa, T. *Analysis of Sterols* 1st edn. (Blackie Academic and Professional Press, London, 1997).
88. Hedges, J. I. & Prahl, F. G. Early diagenesis: consequences for applications of molecular biomarkers. In *Organic Geochemistry, Principles and Applications* (eds Engel, M. H. & Mecko, S. A.) 237–253 (Plenum Press, New York, 1993).
89. Feng, X. & Simpson, M. J. The distribution and degradation of biomarkers in Alberta grassland soil profiles. *Org. Geochem.* **38**, 1558–1570 (2007).
90. Fajardo, A., Gazol, A., Mayr, C. & Camarero, J. J. Recent decadal drought reverts warming-triggered growth enhancement in contrasting climates in the southern Andes tree line. *J. Biogeogr.* **46**, 1367–1379 (2019).
91. Graven, H. *et al.* Compiled records of carbon isotopes in atmospheric CO₂ for historical simulations in CMIP6. *Geosci. Model Dev.* **10**, 4405–4417 (2017).
92. Hayes, J. M. Fractionation of carbon and hydrogen isotopes in biosynthetic processes. *Rev. Miner. Geochem.* **43**, 225–277 (2001).
93. Allen, M. A., Neilan, B. A., Burns, B. P., Jahnke, L. L. & Summons, R. E. Lipid biomarkers in Hamelin Pool microbial mats and stromatolites. *Org. Geochem.* **41**, 1207–1218 (2010).
94. Liu, W. *et al.* Carbon isotope composition of long chain leaf wax *n*-alkanes in lake sediments: a dual indicator of paleoenvironment in the Qinghai-Tibet Plateau. *Org. Geochem.* **83–84**, 190–201 (2015).
95. Westall, F. *et al.* Habitability on Mars from a microbial point of view. *Astrobiology* **13**, 887–897 (2013).
96. Mahaffy, P. R. *et al.* The sample analysis at Mars investigation and instrument suite. *Space Sci. Rev.* **170**, 401–478 (2012).
97. Goesmann, F. *et al.* The Mars organic molecule analyzer (MOMA) Instrument: characterization of organic material in Martian sediments. *Astrobiology* **17**, 655–685 (2017).
98. Siljeström, S. *et al.* Comparison of prototype and laboratory experiments on MOMA GCMS: results from the AMASE11 campaign. *Astrobiology* **14**, 780–797 (2014).
99. Beegle, L. *et al.* SHERLOC: scanning habitable environments with Raman & luminescence for organics & chemicals. In *2015 IEEE Aerospace Conference*, Big Sky, MT, 1–11 (2015).
100. Simoneit, B. R. T., Summons, R. E. & Jahnke, L. L. Biomarkers as tracers for life on early Earth and Mars. *Orig. Life Evol. Biosph.* **28**, 475–483 (1998).
101. Pizzarello, S. *et al.* The nature and distribution of the organic matter in carbonaceous chondrites and interplanetary dust particles. *Meteor. Early Solar Syst.* **II**(1), 625–651 (2006).
102. Georgiou, C. D. & Deamer, D. W. Lipids as universal biomarkers of extraterrestrial life. *Astrobiology* <https://doi.org/10.1089/ast.2013.1134> (2013).
103. Williams, A. J. *et al.* Recovery of fatty acids from mineralogic Mars analogs by TMAH thermochemolysis for the sample analysis at mars wet chemistry experiment on the Curiosity Rover. *Astrobiology* <https://doi.org/10.1089/ast.2018.1819> (2019).
104. Millan, M. *et al.* Lessons learned from the full cup wet chemistry experiment performed on Mars with the Sample Analysis at Mars instrument. In *Ninth International Conference on Mars*, 2019, 22–25 July 2019, Pasadena, CA (2019).

105. Berner, R. A. Biogeochemical cycles of carbon and sulfur and their effect on atmospheric oxygen over Phanerozoic time. *Global Planet. Change* **1**(1–2), 97–122 (1989).
106. Buseck, P. R. & Beyssac, O. From organic matter to graphite: graphitization. *Elements* **10**(6), 421–426 (2014).
107. Mojzsis, S. J. *et al.* Evidence for life on earth before 3,800 million years ago. *Nature* **384**, 55–59 (1996).
108. Ohtomo, Y., Kakegawa, T., Ishida, A., Nagase, T. & Rosing, M. T. Evidence for biogenic graphite in early Archaean Isua meta-sedimentary rocks. *Nat. Geosci.* **7**, 25–28 (2014).
109. Breuer, D. & Spohn, T. Early plate tectonics versus single-plate tectonics on Mars: evidence from magnetic field history and crust evolution. *J. Geophys. Res.: Planets* <https://doi.org/10.1029/2002JE001999> (2003).
110. Rampe, E. B. *et al.* Mineralogy and geochemistry of sedimentary rocks and eolian sediments in Gale crater, Mars: a review after six Earth years of exploration with curiosity. *Geochemistry* <https://doi.org/10.1016/j.chemer.2020.125605> (2020).
111. Borlina, C. S., Ehlmann, B. L. & Kite, E. S. Modeling the thermal and physical evolution of Mount Sharp's sedimentary rocks, Gale Crater, Mars: implications for diagenesis on the MSL Curiosity rover traverse. *J. Geophys. Res.: Planets* **120**(8), 1396–1414 (2015).
112. Nachon, M. *et al.* Calcium sulfate veins characterized by ChemCam/Curiosity at Gale crater, Mars. *J. Geophys. Res.: Planets* **119**, 1991–2016 (2014).
113. Nachon, M. *et al.* Chemistry of diagenetic features analyzed by ChemCam at Pahrump Hills, Gale crater, Mars. *Icarus* **281**, 121–136 (2017).
114. Sun, V. Z. *et al.* Late-stage diagenetic concretions in the Murray formation, Gale crater, Mars. *Icarus* **321**, 866–890 (2019).
115. Hassler, D. M. *et al.* Mars' surface radiation environment measured with the Mars Science Laboratory's Curiosity rover. *Science* **343**(6169), 1244797 (2014).
116. Ehlmann, B. L. & Edwards, C. S. Mineralogy of the Martian surface. *Annu. Rev. Earth Planet. Sci.* **42**, 291–315 (2014).
117. Vaniman, D. T. *et al.* Mineralogy of a mudstone at Yellowknife Bay, Gale crater, Mars. *Science* **343**(6169), 1243480 (2014).
118. Fairén, A. G. A cold and wet Mars. *Icarus* **208**, 165–175 (2010).
119. Bishop, J. L. *et al.* Surface clay formation during short-term warmer and wetter conditions on a largely cold ancient Mars. *Nat. Astron.* **2**, 206–213 (2018).
120. Warren-Rhodes, K. A. *et al.* Subsurface microbial habitats in an extreme desert Mars-analog environment. *Front. Microbiol.* **10**, 69 (2019).
121. Warren-Rhodes, K. *et al.* Robotic ecological mapping: habitats and the search for life in the Atacama Desert. *J. Geophys. Res. Biogeosci.* **112**, G04S06 (2007).
122. Yen, A. S. *et al.* Multiple stages of aqueous alteration along fractures in mudstone and sandstone strata in Gale Crater, Mars. *Earth Planet. Sci. Lett.* **471**, 186–198 (2017).
123. Hausrath, E. M., Ming, D. W., Peretyazhko, T. S. & Rampe, E. B. Reactive transport and mass balance modeling of the Stimson sedimentary formation and altered fracture zones constrain diagenetic conditions at Gale crater, Mars. *Earth Planet. Sci. Lett.* **491**, 1–10 (2018).
124. Fairén, A. G. *et al.* Planetary protection and the astrobiological exploration of Mars: proactive steps in moving forward. *Adv. Space Res.* **63**, 1491–1497 (2019).
125. Drever, J. I. The preparation of oriented clay mineral specimens for X-ray diffraction analysis by a filter-membrane peel technique. *Am. Miner.* **58**, 553–554 (1973).
126. Frost, R. L. & Johansson, U. Combination bands in the infrared spectroscopy of Kaolins-A drift spectroscopic study. *Clays Clay Miner.* **46**, 466–477 (1998).
127. Herlemann, D. P. *et al.* Transitions in bacterial communities along the 2000 km salinity gradient of the Baltic Sea. *ISME J.* **5**, 1571–1579 (2011).
128. Schloss, P. D. *et al.* Introducing mothur: open-source, platform-independent, community-supported software for describing and comparing microbial communities. *Appl. Environ. Microbiol.* **75**, 7537–7541 (2009).
129. Kozich, J. J., Westcott, S. L., Baxter, N. T., Highlander, S. K. & Schloss, P. D. Development of a dual-index sequencing strategy and curation pipeline for analyzing amplicon sequence data on the MiSeq illumina sequencing platform. *Appl. Environ. Microbiol.* **79**, 5112–5120 (2013).
130. Cole, J. R. *et al.* Ribosomal database project: data and tools for high throughput rRNA analysis. *Nucleic Acids Res.* **42**, D633–D642 (2013).
131. Edgar, R. C. MUSCLE: multiple sequence alignment with high accuracy and high throughput. *Nucleic Acids Res.* **32**, 1792–1797 (2004).
132. Posada, D. jModelTest: phylogenetic model averaging. *Mol. Biol. Evol.* **25**, 1253–1256 (2008).
133. Felsenstein, J. PHYLIP (*phylogeny inference package*) version 3.6. *Distributed by Author*. Department of Genome Sciences, University of Washington, Seattle. (2005)
134. Ramirez-Flandes, S. & Ulloa, O. Bosque: integrated phylogenetic analysis software. *Bioinformatics* **24**, 2539–2541 (2008).
135. Bartosch, S., Mansch, R., Knötzsch, K. & Bock, E. CTC staining and counting of actively respiring bacteria in natural stone using confocal laser scanning microscopy. *J. Microbiol. Methods* **52**, 75–84 (2003).
136. Sánchez-García, L. *et al.* Microbial biomarker transition in El Tatio (Chile) sinter mounds through different stages of hydro-thermal activity. *Front. Microbiol.* **9**, 3350 (2019).
137. Singleton, G.L., Révész, K. & Coplen, T.B. Determination of the $\delta^{13}\text{C}$ of dissolved inorganic carbon in water; RSIL Lab Code 1710. In *Stable Isotope Ratio Methods, sec. C of Methods of the Reston Stable Isotope Laboratory* (eds Révész, K. & Coplen, T. B.). U.S. Geological Survey Techniques and Methods, book 10 (2012), pp. 1–28

Acknowledgements

The reported research is a contribution from the Project “MarsFirstWater”, funded by the European Research Council, ERC Consolidator Grant No. 818602 to AGF and by the Human Frontiers Science Program grant n° RGY0066/2018 to AAB. This work was also supported by the grant PGC2018-094076-B-I00 to JW and CA from the Ministry of Science, Innovation and Universities of Spain.

Author contributions

A.A-B. designed the research strategy. A.G.F. and E.B.R. placed the Atacama results in the context of current Mars exploration. A.A-B. and C.G-S. conducted the sampling and the microbiological and molecular biology experiments. M.A.F. analyzed NGS sequences. M.F-S. performed XRD analysis. D.C. and L.S-G. performed biosignature analyses. C.G-L. identified clay mineral species. C.A-F. performed all statistical analyses. J.W. and C.A. performed cell staining and fluorescence microscopy of the clay mineral samples. A.A-B., A.G.F., and E.B.R. wrote the manuscript.

Competing interests

The authors declare no competing interests.

Additional information

Supplementary information is available for this paper at <https://doi.org/10.1038/s41598-020-76302-z>.

Correspondence and requests for materials should be addressed to A.A.-B. or A.G.F.

Reprints and permissions information is available at www.nature.com/reprints.

Publisher's note Springer Nature remains neutral with regard to jurisdictional claims in published maps and institutional affiliations.



Open Access This article is licensed under a Creative Commons Attribution 4.0 International License, which permits use, sharing, adaptation, distribution and reproduction in any medium or format, as long as you give appropriate credit to the original author(s) and the source, provide a link to the Creative Commons licence, and indicate if changes were made. The images or other third party material in this article are included in the article's Creative Commons licence, unless indicated otherwise in a credit line to the material. If material is not included in the article's Creative Commons licence and your intended use is not permitted by statutory regulation or exceeds the permitted use, you will need to obtain permission directly from the copyright holder. To view a copy of this licence, visit <http://creativecommons.org/licenses/by/4.0/>.

© The Author(s) 2020